Contribution of Floquet-Bloch states to high-order harmonic generation in solids

Jian-Zhao Jin,[1,*] Hao Liang,[1,*] Xiang-Ru Xiao,[1] Mu-Xue Wang,[1] Si-Ge Chen,[1] Xiao-Yuan Wu,[1] Qihuang Gong,[1,2,3] and Liang-You Peng[1,2,3,†]

[1]*State Key Laboratory for Mesoscopic Physics and Collaborative Innovation Center of Quantum Matter, School of Physics, Peking University, Beijing 100871, China*

[2]*Beijing Academy of Quantum Information Sciences, Beijing 100193, China*

[3]*Collaborative Innovation Center of Extreme Optics, Shanxi University, Taiyuan, Shanxi 030006, China*

(Received 14 November 2018; revised manuscript received 2 May 2019; published 16 July 2019)

We identify the contribution of Floquet-Bloch states to the high-order harmonic generation (HHG) in solids by numerically solving the time-dependent Schrödinger equation for both a one-dimensional and a two-dimensional model. Results from the single k point and the full Brillouin zone are compared to each other and the symmetry-breaking effect is discussed. We show that the observed phenomena can be explained under the framework of the Floquet-Bloch theory and the strong-field approximation, respectively. Our results indicate that the total yield of the harmonic radiation increases nonmonotonically with the intensity of the driving pulse. After a rough consideration of the focusing volume effects, we find that the yield of the harmonics shows a steplike structure, which is similar to several recent experimental observations. The present work can contribute to a better understanding of the channel-closing effect in the HHG of solids and may provide a way to detect the Floquet-Bloch bands in a laser field.

DOI: 10.1103/PhysRevA.100.013412

I. INTRODUCTION

In the past few years, high-order harmonic generation (HHG) in solids shined by strong laser pulses has attracted great attention since its experimental observation [1–4]. HHG in semiconductors can be used to study the dynamics of the electron on ultrafast timescales [3] and to explore the properties of energy bands in solids [4–6]. Recent experimental measurements have been carried out for two-dimensional (2D) materials such as graphene [7,8] and magnetic materials [9].

The time-dependent Schrödinger equation [10,11], the semiconductor Bloch equation [12–14], and the time-dependent density function theory [15] are the main theoretical methods to study the HHG in solids. The advantages and disadvantages of these methods have been discussed [16]. There used to be a debate between the interband and the intraband transition mechanisms for HHG in solids [1,10, 17–20], which comes from the momentum-dependent gap energy and band nonparabolicity, respectively. Now it seems that a consensus has been reached that both mechanisms coexist to give a first cutoff which linearly scales with the electric-field strength of a laser pulse. Apart from the two-band models, the electron can actually be excited to higher conduction bands when the laser intensity is further increased. Under this circumstance, many energy bands should be considered in the generation of harmonics [11,21]. It has been shown that the interband transitions between multiple bands play an essential role in the harmonic radiation [21–24], e.g., multiple plateaus have been observed. The orientation and ellipticity dependence of HHG in solids have been recently observed experimentally [4,25–29] and discussed theoretically [30–33]. In addition, the HHG can be controlled by the carrier-envelope phase (CEP) of the driving pulse [26,34], which demonstrates a potential way to the subcycle control of the electron dynamics in crystals.

The systems of a crystalline structure interacting with a monochromatic laser field can be studied by using the Floquet-Bloch theory since they are both spatially and temporally periodic. Faisal and Genieser used the Floquet-Bloch theory to show the exact dispersion relation for the Krönig-Penney model [35]. By studying the modification of the laser-modified band structure, they also predicted that a semiconductor medium is more efficient in generating high-order harmonics than either an insulator or a metal film, which has been confirmed in recent experiments [1,2]. They also used the Floquet analysis to predict the formation of a plateau structure existing in both the photocurrent and the spectrum of the HHG radiation at the surface of solid. Alon and co-workers used a space-time system to characterize the modifications of the electron energy levels induced by circularly polarized laser fields in quantum rings, thin crystals, and carbon nanotubes [36]. Tight-binding models combined with the Floquet theory have been widely used to analyze the Floquet-Bloch shift of the band structure [37] and the blueshift of the band edge [38], and the dynamic symmetry based on the selection rules in the graphite system [39]. Park investigated the interference between the Floquet states and laser-assisted photoemission effect during the photoemission [40].

Experimentally, Wang and co-workers observed the Floquet-Bloch bands in solids by using time- and angle-resolved photoemission spectroscopy [41]. This pump-probe

*These authors equally contribute to this work.
†liangyou.peng@pku.edu.cn

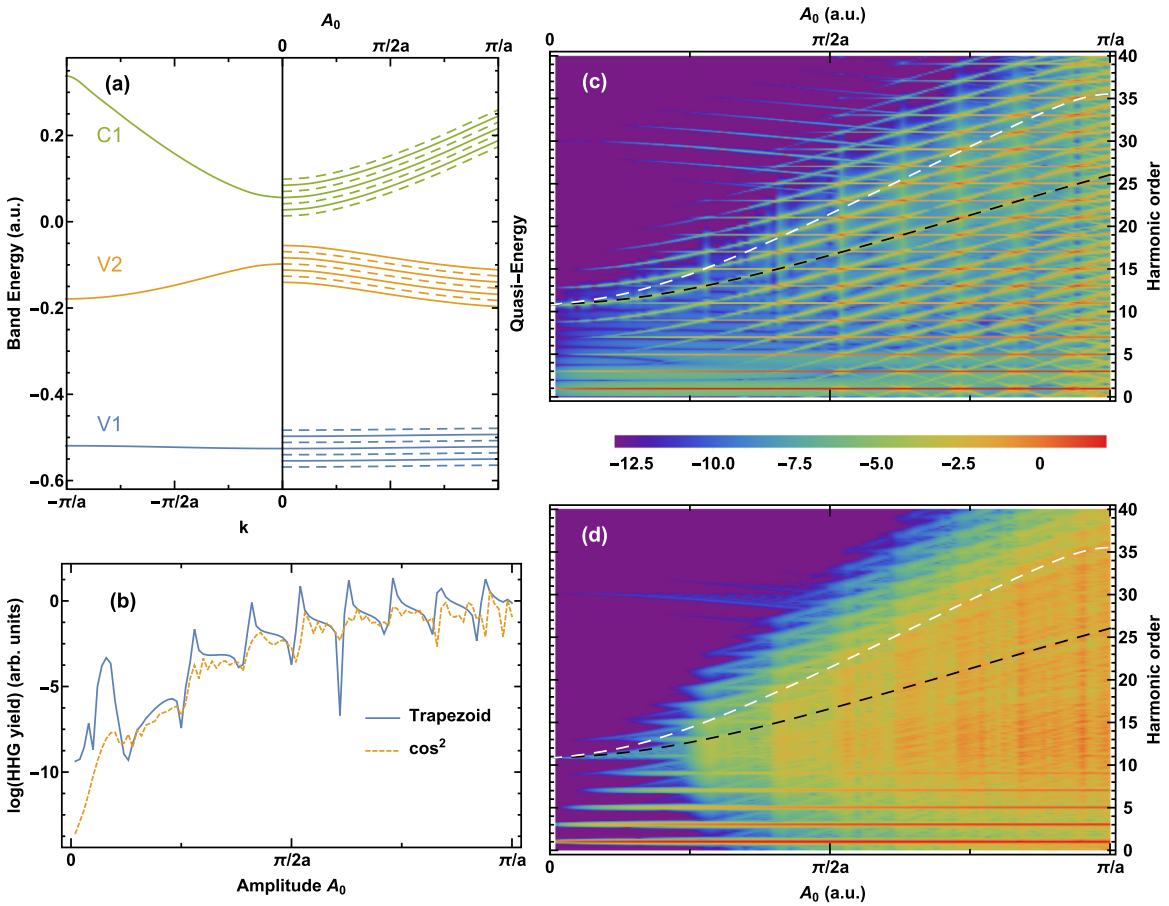

FIG. 1. (a) Left panel: the first three energy bands of the one-dimensional model. Right panel: the corresponding quasienergies as a function of the amplitude of the vector potential. The solid lines and dashed lines represent states with different parities. (b) The yield of the 11th-order harmonic induced by a trapezoidal (blue solid line) and cosine square (yellow dashed line) envelope at various A_0. The full HHG spectrum is, respectively, shown in (c) for the trapezoidal envelope and (d) for the cosine square envelope. The black dashed line and white dashed line are $\Omega_{C1}(A_0) - \Omega_{V2}(A_0)$ and $E_{C1}(A_0) - E_{V2}(A_0)$, respectively.

method has been frequently used to study the Floquet-Bloch states. One can use the absorption spectrum of the probe laser pulse to examine the modification of the band structure, which is caused by the interaction with the pump laser pulse.

In the present work, we will mainly focus on the harmonics induced by a quasimonochromatic midinfrared laser field. By varying the peak intensity of the laser pulse, we identify resonance peaks in the spectrum. This phenomenon is caused by the resonance enhancement between different Floquet-Bloch states. Then we use all k points from the full Brillouin zone (BZ) to calculate the high-order harmonic generation, in which case we find the channel-closing effect, analog to that in the atomic systems. By applying a rough focusing volume averaging of the laser pulse, we observe steplike structures in the harmonic yield as a function of the laser intensity, which may explain similar phenomena observed in recent experiments [1,6,28,42].

The rest of the paper is organized as follows. We start with our basic observation of the contributions of the Floquet-Bloch states to the harmonic generation in a one-dimensional model. Then we provide two theoretical frameworks to understand and calculate the observed phenomena. Finally, we present our main results and discussions, including the comparisons between the results from different theoretical methods, the consideration of all the k points in the full BZ, the generation to a two-dimensional model, and the averaging over the focusing volume.

II. BASIC OBSERVATION

Let us start with our basic observation from a 1D model, which has been used in our previous work to discuss the Michelson interferometry of high-order harmonic generation in solids [43]. In this model, the periodic potential is taken to be

$$V(x) = V_0\left(1 + \cos\frac{2\pi x}{a}\right), \tag{1}$$

where $V_0 = -0.37$ a.u. and the lattice constant of the crystal $a = 8$ a.u. The lowest three energy bands are shown in the left part of Fig. 1(a), where one has two valence bands (V_1, V_2) and one conduction band C_1. The laser-matter interaction is described in the velocity gauge under the dipole approximation, with the vector potential of the laser pulse given by

$$A(t) = A_0 f(t)\cos(\omega_0 t), \tag{2}$$

where A_0, $f(t)$, and ω_0, respectively, stands for the peak vector potential, the pulse envelope, and the central angular frequency.

The corresponding time-dependent Schrödinger equation (TDSE) can be easily solved [24,43]. For a clear demonstration of the contribution of Floquet-Bloch states to HHG, we first choose the V_2 as the initial state and temporally consider the transition from a single point at $k = 0$. In Fig. 1(c), we present the harmonic spectrum as a function of the peak vector potential A_0 for an eight-cycle laser pulse with $\omega_0 \approx 0.014$ a.u. ($\lambda = 3200$ nm) and $f(t)$ being trapezoidal with one cycle ramp on and one cycle ramp off. The peak intensity of the pulse is given by $I_0 = \omega_0^2 A_0^2$. As can be seen, the spectrum shows two set of structures: the horizontal ones being the usual odd harmonics and the unexpected slanted fringes. The latter intensity-dependent fringes remind us of the channel-closing effect in the atomic ionization due to the U_p shift (see, e.g., [44]).

To check this speculation, we calculate the time-averaged energy difference $\overline{\Delta E}$ within one optical cycle and plot it in Fig. 1(c) with a black dashed line as a function of A_0, which indeed coincides perfectly with one of the the slanted fringes. In addition, one notices that all of these slanted curves are "parallel" to each other and are separated by $2\omega_0$. For harmonic orders greater than about 27, there also exist weak slanted fringes but with negative slopes [see, e.g., the left-upper quarter of Fig. 1(c)], which can be explained with a similar mechanism from the Floquet-Bloch states but for the transitions between the two valence bands V_1 and V_2.

One may wonder whether these slanted fringes can be simply described by the simple classical prediction of HHG cutoff from the interband transition model. We thus plot $\Delta E(A_0)$ as a white dashed line in Fig. 1(c). As a fact, it does not follow the trend of the slanted curves, while it only qualitatively gives a rough prediction of the cutoff with the increase of A_0.

Due to the contributions of the Floquet-Bloch states, the yield of harmonics at a particular order would not monotonically increase with the pulse intensity. Significant enhancement can be clearly seen near the crossing points of the two sets of the structures in Fig. 1(c). To quantitatively examine this enhancement, it is instructive to plot the harmonic yield of a particular order as a function of the peak value A_0 of the vector potential. In Fig. 1(b), we show the yield of the 11th harmonics (the solid blue line) by integrating over a width of ω_0 around the energy of $11\omega_0$ from the data shown in Fig. 1(c). Indeed, one can observe that the HHG yield increases nonmonotonically with the increase of the vector potential A_0 and asymmetric Fano-type resonance peaks are present, which indicates the existence of resonance behavior of the discrete and continuous states.

Finally, it is important to check whether the above observation from a trapezoidal pulse persists with other types of pulse envelope. We thus change $f(t)$ into a cosine square shape, but with all other parameters kept the same. The harmonic spectrum is shown in Fig. 1(d), from which one can see that those slanted structures do appear, although not as distinct as those for the trapezoidal pulse. Most importantly, as shown in Fig. 1(b) with a dashed line, the integrated yield for the 11th order also shows steplike resonance structures.

III. THEORETICAL DESCRIPTION

In this section, we formulate the theoretical framework to understand the observed structures in the harmonic spectrum. The dynamics of the quasielectron can be described by the time-dependent Schrödinger equation in the Houston basis [10],

$$i\dot{a}_i(t) = E_i[k(t)]a_i(t) + F(t)\sum_j \xi_{ij}[k(t)]a_j(t), \tag{3}$$

in which $a_i(t)$ is the occupation probability amplitude of the Bloch state in the ith band and $E_i(k)$ is the corresponding band energy with a quasimomentum $k(t) = k_0 + A(t)$, $F(t) = -\partial_t A(t)$ is the electric field of the applied laser pulse, and the dipole transition matrix between different bands is given by

$$\xi_{ij}(k) = i\langle\Psi_i(k)|\nabla_k|\Psi_j(k)\rangle, \tag{4}$$

where $\Psi_i(k)$ is the Bloch wave function of the single-electron Hamiltonian H. In order to calculate the HHG spectrum, the first step is to evaluate the expectation value of the momentum operator,

$$p_{ij}(k) = \langle\Psi_i(k)|\nabla_k H|\Psi_j(k)\rangle. \tag{5}$$

In the following, we will present two approximate approaches, which will help us to interpret the observed structures in the harmonic spectra.

A. Floquet-Bloch approach

Considering a monochromatic laser field with a frequency ω_0, one notices that Eq. (3) is periodic in time. Therefore, we can expand the wave function in terms of the Floquet states, i.e.,

$$|a(t)\rangle = \sum_\alpha b_\alpha e^{-i\Omega_\alpha t}|u_\alpha(t)\rangle, \tag{6}$$

where Ω_α is the Floquet frequency. Since the corresponding Floquet state $u_\alpha(t)$ is also periodic in time, it can be further expanded into Fourier series,

$$|u_\alpha(t)\rangle = \sum_{n\in\mathbb{Z}} |u_{\alpha,n}\rangle e^{in\omega_0 t}. \tag{7}$$

It should be noted that $e^{-im\omega_0 t}|u_\alpha(t)\rangle$ is still the Floquet state of the system with the Floquet frequency $\Omega_\alpha + m\omega_0$, $m \in \mathbb{Z}$.

For the convenience and clarity of the theoretical analysis, we only consider two bands, $i = c, v$, e.g., the C_1 and V_2 band as shown in the left part of Fig. 1(a). We use the same subscription c, v to denote the Floquet state. The current can be evaluated as

$$\begin{aligned} j(t;k_0) &\propto \sum_{ij} a_i^*(t)p_{ij}(k(t))a_j(t) \\ &= \sum_{\alpha=c,v}|b_\alpha|^2\sum_{n,m,l}\langle u_{\alpha,n}|\hat{p}_l|u_{\alpha,m}\rangle e^{-i(m-n+l)\omega_0 t} \\ &\quad + 2\mathrm{Re}\left[b_v^* b_c \sum_{n,m,l}\langle u_{v,n}|\hat{p}_l|u_{c,m}\rangle e^{-i[\Omega_c-\Omega_v+(m-n+l)\omega_0]t}\right], \end{aligned} \tag{8}$$

where $\hat{p}_l$ is the Fourier component of $\hat{p}(k(t))$, i.e., $\hat{p}(k(t)) = \sum_l \hat{p}_l e^{-il\omega_0 t}$, $l \in \mathbb{Z}$.

For a system with a space reflection symmetry, $\hat{p}_l \neq 0$ only for l being even, $\langle u_{\alpha,n} \mid \hat{p}_l \mid u_{\alpha,m}\rangle$ vanishes for all even $(m-n)$, and $\langle u_{v,n} \mid \hat{p}_l \mid u_{c,m}\rangle$ vanishes for all odd $(m-n)$. Thus, the Fourier transform of the current can be simplified to be

$$\tilde{j}(\omega) \propto \sum_l \beta_l \delta[(2l+1)\omega_0 - \omega] + \sum_l \gamma_l \delta[\Omega_c - \Omega_v + 2l\omega_0 - \omega], \tag{9}$$

in which the first term represents the usual odd harmonics, while the second term can be interpreted as transitions between the different Floquet-Bloch states. It is obvious that Ω_α depends on the amplitude of the vector potential of the laser pulse. Therefore, if one plots the yield of a certain harmonic $\omega = (2l+1)\omega_0$ as a function of the field strength, one may observe Fano-type resonance peaks satisfying $\Omega_c - \Omega_v = (2l+1-2l')\omega_0$, embedded in the continuum [45].

For laser pulses in the low-frequency limit, i.e., $|F\xi_{cv}| \ll E_c - E_v$ but with the vector potential still comparable with the reciprocal lattice vector π/a, the Floquet states can be approximated into the zeroth order,

$$\langle \Psi_i(k) | u_\alpha^{(0)}(t)\rangle = \delta_{i,\alpha} \exp\left[i\Omega_\alpha^{(0)} t - i\phi_i(t)\right], \tag{10}$$

where $\phi_i(t) = \int_0^t E_i[k(t)]dt$ is the dynamical phase and $\Omega_\alpha^{(0)} = \phi_i(T)/T$ is the corresponding Floquet frequency with $T = 2\pi/\omega_0$. With these results in mind, we can now attribute the slanted fringes present in Fig. 1(c) to the transitions between various Floquet-Bloch states with different parities. The energies of these Floquet states in the zeroth order are shown in the right part of Fig. 1(a).

For a monochromatic laser field, it is possible to diagonalize Eq. (3) with the concept of Floquet states [46]. However, it is not straightforward to do so for a realistic laser pulse with an envelope $f(t)$. This is because, in the low-frequency limit considered here, level crossings $\Omega_c^{(0)} - \Omega_v^{(0)} = (2l+1)\omega_0$ will happen for many times, which breaks the adiabatic condition for the Floquet state population $\{b_\alpha\}$ even for a slowly varying envelope [47]. To resolve this problem, one can turn to the strong-field approximation, which will be detailed in the next section.

B. Strong-field approximation

The picture of strong-field approximation (SFA) [18,20] has been useful in the qualitative understanding of the HHG in solids. In the following, we will derive a semianalytical formula which can quantitatively describe the harmonic yield, in principle, for a laser pulse with an arbitrary envelope $f(t)$.

Without considering the depletion effect of the valence band (i.e., $|a_c|^2 \ll |a_v|^2$), the approximate solution to Eq. (3) can be expressed as

$$a_v(t) = e^{-i\phi_v(t)} \int_{-\infty}^{t} F(\tau)\xi[k(\tau)] e^{-i\phi_{cv}(\tau)} d\tau. \tag{11}$$

Due to the fact that $e^{-i\phi_{cv}(t)} = e^{i[\phi_v(t) - \phi_c(t)]}$ is a fast oscillating function, the above integration is mainly contributed at the vicinity of the saddle points,

$$\frac{d}{dt}\phi_{cv}(t)|_{t=t_s} = E_v[k(t_s)] - E_c[k(t_s)] = 0. \tag{12}$$

Apparently, similar to the atomic case [48–51], there is no root for Eq. (12) if one restricts $t_s \in \mathbb{R}$. Therefore, we have to extend to the complex plane of time $t_s = t_r + it_i$. Only the roots in the lower-half plane with $t_r < t$ need to be considered, and the result of Eq. (11) is given by summing over all those saddle points, i.e.,

$$a_v(t) \approx e^{-i\phi_v(t)} \sum_{\mathrm{Re}\, t_s < t} \mathrm{sgn}[F(t_s)\xi_{cv}] e^{-i\phi_{cv}(t_s)}, \tag{13}$$

whose details of derivation can be found in the Appendix. Equation (13) can be interpreted as the tunneling from the valence band to the conduction band at time $\mathrm{Re}\, t_s$ with probability $e^{2\,\mathrm{Im}\,\phi_{cv}(t_s)}$ and phase $-\mathrm{Re}\,\phi_{cv}(t_s)$. We can now evaluate the yield of HHG according to the Fourier transform of the interband current,

$$j_{\mathrm{inter}}(t) = 2\,\mathrm{Re}\left\{ p_{cv}[k(t)] e^{i\phi_{cv}(t)} \sum_{\mathrm{Re}\, t_s < t} \mathrm{sgn}[F(t_s)] e^{-i\phi_{cv}(t_s)} \right\}. \tag{14}$$

As an example, let us consider the case of a monochromatic pulse and a single point $k_0 = 0$. There are two instances of tunneling per optical cycle, which corresponds to $A(t_r) = 0$. Since the direction of electric field is opposite, the phase difference between these two tunneling events is $\Delta\phi = -\phi_{cv}(T/2) + \pi$. If the constructive interference condition $\Delta\phi = 2l\pi$ is satisfied, i.e., $\Omega_c^{(0)} - \Omega_v^{(0)} = (2l+1)\omega_0$, there will be an efficient population transfer from the valence band to the conduction band, i.e., the resonance enhancement occurs, as shown in Fig. 2(a1). In this case, all orders of HHG will be enhanced. Wismer *et al.* [52] found this type of interference in the region of photon energy ω_0 close to energy gap Δ theoretically, and investigated its effect on field-induced current. Paasch-Colberg *et al.* [53] and Du *et al.* [54,55] also noticed this in the region of $\omega_0 \ll \Delta$ and regarded it as a subcycle interference.

For the off-resonance case, the geometric series can be easily summed up as below,

$$j_{\mathrm{inter}}(t) = 2\,\mathrm{Re}\, p_{cv}[k(t)] e^{i\phi_{cv}(t)} \frac{1 - \exp(iN\Delta\phi)}{1 - \exp(i\Delta\phi)} e^{\mathrm{Im}\,\phi_{cv}(t_s)}, \tag{15}$$

where N is the number of saddle points satisfying $\mathrm{Re}\, t_s < t$. It can be shown that the current can be divided into two quasiperiodic parts: by a time translation of $T/2$, the first part has a phase change of $(\Omega_c^{(0)} - \Omega_v^{(0)})T/2$, while the second part only changes the sign. One can get an intuitive understanding by examining Fig. 2(a2). From these arguments in the framework of SFA, one can rediscover Eq. (9), which has been derived in the Floquet-Bloch picture: the usual odd-order harmonics $\omega = (2l+1)\omega_0$ and the intensity-dependent slanted fringes for $\omega = 2l\omega_0 + \Omega_v^{(0)} - \Omega_c^{(0)}$. With the help of

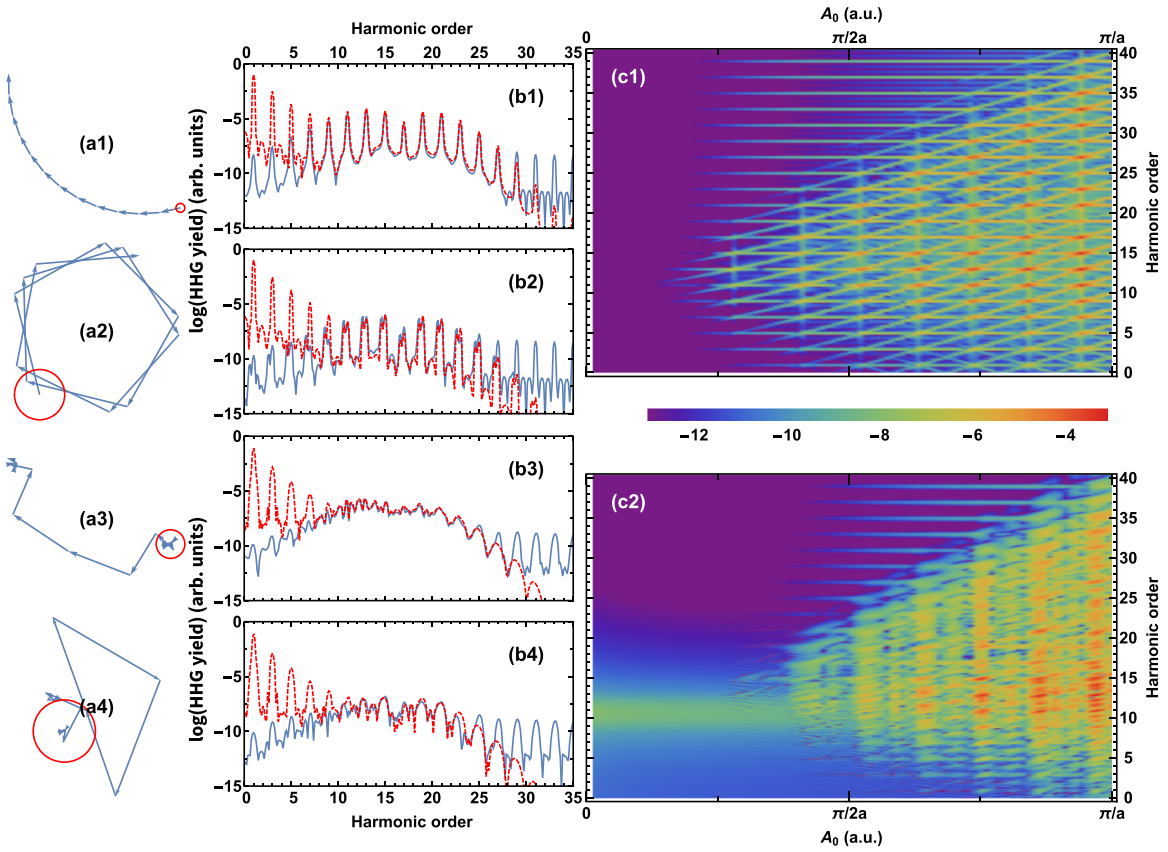

FIG. 2. The harmonic spectra calculated by SFA at different peak vector potential A_0 of laser pulses with a trapezoidal or cosine square envelope. (a1)–(a4) The amplitude of the conduction band for the laser pulse: (a1) a trapezoidal pulse with $A_0 = 0.52\pi/a$, (a2) a trapezoidal pulse with $A_0 = 0.50\pi/a$, (a3) a cosine square pulse with $A_0 = 0.52\pi/a$, and (a4) a cosine square pulse with $A_0 = 0.50\pi/a$. In these four subfigures, the red circle centered at the origin has the same absolute size to indicate the scale and the small arrows represent the tunneling amplitude in each saddle point. (b1)–(b4) The corresponding HHG spectra, calculated by TDSE (red dashed line) and by SFA (blue solid line). (c1),(c2) An overview of the HHG spectra calculated by SFA as a function of A_0 for (c1) a trapezoidal pulse and (c2) a cosine square pulse.

the saddle-point method, it is much easier to compute the harmonic spectrum for an arbitrary laser pulse.

IV. RESULTS AND DISCUSSIONS

In the last two sections, we have presented the observed HHG features contributed by the Floquet-Bloch states and two theoretical frameworks to understand them. In this section, we will carry out detailed comparisons between the numerical results calculated by TDSE and those by SFA to reveal the underlying mechanism.

We will first continue to discuss the situation for the 1D model, starting from a single point $k_0 = 0$. Then we will present the overall HHG yield, summed over the whole BZ. In the latter case, the contribution by the Floquet-Bloch states is still observed, but with a weaker intensity, and becomes spaced by $1\omega_0$ instead of $2\omega_0$ due to the breaking of the symmetry. Finally, it is important to check whether the observed features in the HHG spectra are still present for a two-dimensional model. As will be shown, with the same mechanism, they do appear in the more realistic two-dimensional model, even when one considers the total yield from the whole BZ. Again, if one examines the harmonic yield of a particular order, it shows a steplike structure as a function of the laser peak intensity.

A. Comparisons between SFA and TDSE

Let us start with a comparison study for the 1D model by the SFA method and the TDSE. At the moment, we restrict the calculation to the single point $k_0 = 0$. For the trapezoidal pulse used previously, in Fig. 2(c1), we plot the full HHG spectra evaluated by SFA as a function of A_0. As one can see, the SFA results reproduce all the main distinct features observed in Fig. 1(c), i.e., the odd-order harmonics and the slanted fringes contributed by the Floquet-Bloch states.

For a quantitative comparison, in Figs. 2(b1) and 2(b2), we plot the harmonic yield at $A_0 = 0.52\pi/a$ and $0.50\pi/a$, respectively. Odd-order harmonics are clearly shown in Fig. 2(b1), while each peak is split into two in Fig. 2(b2). Actually, the choice of the A_0, respectively, corresponds to a near-resonance and an off-resonance case. It can be seen that for both cases, the results from SFA agree well with those from TDSE in the plateau region. Nevertheless, SFA underestimates the yield in the lower-order harmonics and overestimates in the higher-order ones. The differences in both regions can be understood since lower-order harmonics are dominated by the intraband current [10,18,56,57] which is not considered in Eq. (14). At the same time, the integration (11) is approximated as a discrete summation, which results in the unphysical high-frequency Fourier components.

Similar comparisons between SFA and TDSE can be made for a more realistic pulse envelope, i.e., a cosine square $f(t) = \cos^2(\omega_0 t/2N)$, where $N = 8$ is the number of optical cycles. As can been seen from Figs. 2(b3), 2(b4), and 2(c2), overall agreement has been achieved with those of TDSE, which confirms the reliability of the present SFA method.

In Figs. 2(a1)–2(a4), we plot each term in the series given by Eq. (14) as a list of connected vectors, respectively, for the corresponding pulse shape and the peak vector potential. For the latter case of the cosine square shape, it can be noticed that the population transfer is dominated by the 4–6 saddle points in the middle of the pulse, which agrees with the exponential dependence of the tunneling probability on the instant field strength. In this region of time, the phase term ϕ_{cv} is roughly the same for different pulse envelopes. This explains the similar near-resonance and off-resonance behavior in both cases of pulse shapes, although slightly more irregular for the case of the cosine square shape. It indicates the origin of the noisy feature in the plateau region of Figs. 2(b3) and 2(b4), which has been previously observed by TDSE calculations [18,23,58]. However, for the cosine square case, the overall spectra as a function of A_0 [cf. Fig. 2(c2)] show clear patterns, similar to the trapezoidal case.

B. Integrated yield over the full BZ

In the previous sections, the discussions have been restricted to calculations from a single k point. Indeed, many TDSE calculations based on the models from a single k point have succeeded in interpreting many properties of HHG experimentally observed in solids. For example, the cutoff was found to be linearly dependent on the laser wavelength and the field strength, instead of a quadratic scaling for the atomic case [10]. In addition, the second plateau was observed and explained in the solid Ar and Kr [4,11]. However, for a realistic solid material, the quasielectron is in the full valence band, instead of only staying at the top of it. Moreover, recent studies have shown some limitation of the single k point models in examining the HHG yield dependence on the wavelength or the electric-field strength [59].

In the present study of the contributions of the Floquet-Bloch states, it will be instructive to check the influences if one calculates the total current for all k points from the highest valence band. Then, we use the summed current from all the points to extract the signal of harmonic radiation.

For the 1D model which we have considered in Sec. II, we calculate the harmonic spectra from all the k points in the V_2 band. By summing the current over the full BZ, the final results are shown as a function of A_0 in Figs. 3(a) and 3(b), for the trapezoidal and the cosine square envelope, respectively. All the laser parameters are kept the same with those used in Figs. 1(c) and 1(d). As can be seen from Fig. 3(a), for the trapezoidal pulse, the signals for the usual odd-order harmonics are still strong, while the slanted fringes originally with a $2\omega_0$ spacing change to be spaced by $1\omega_0$ with a significantly lower intensity. The overall enhancement at the crossing points of two sets of structures can still be clearly observed in Fig. 3(a). Actually, the positions of these enhancements roughly coincide with those in the result of the single k point shown in Fig. 1(c).

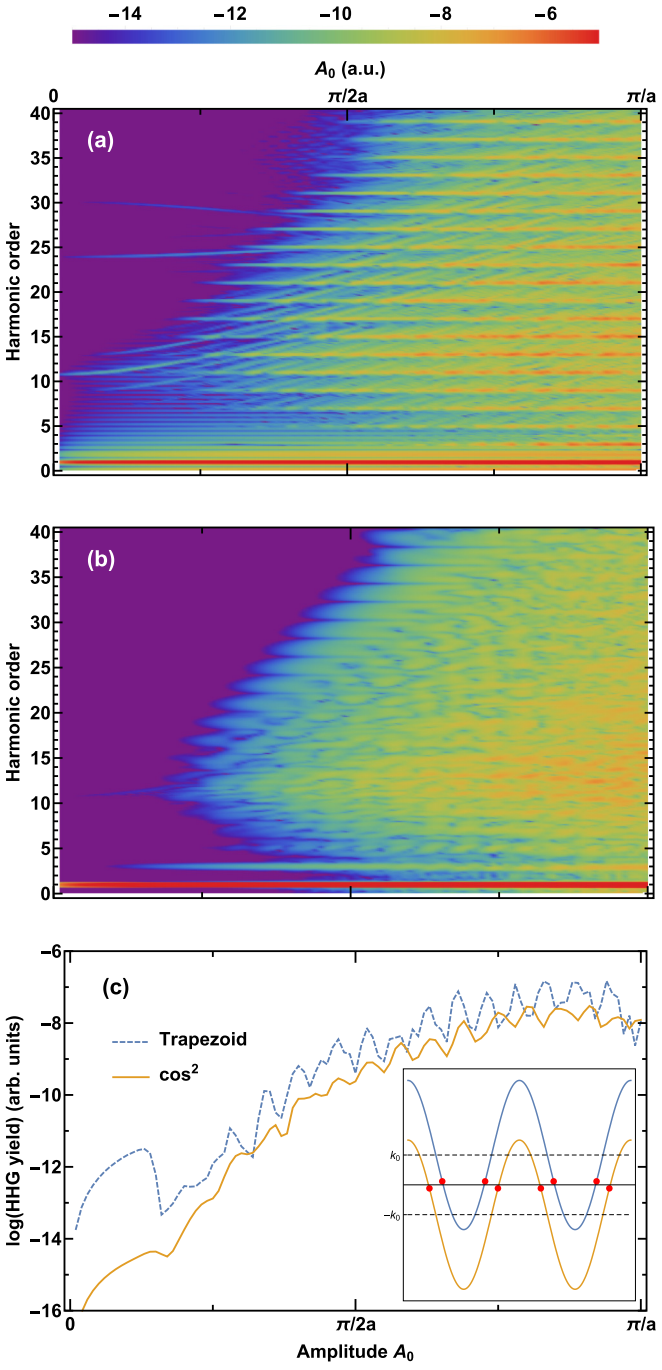

FIG. 3. The full HHG spectrum integrated over the full BZ calculated by TDSE for (a) the trapezoidal envelope and (b) the cosine square envelope. (c) The yield of 11th-order harmonics as a function of peak vector potential. Other parameters are the same as those in Fig. 1. The SFA results (not shown here) agree with the TDSE calculation quantitatively in the plateau region. The inset in (c) shows the momentum-space trajectory for electrons starting from $k_0 > 0$ (blue line) and from $-k_0$. The red points represent the saddle points.

When the pulse shape changed into a cosine square, the slanted fringes are hard to identify, as shown in Fig. 3(b). However, the intensity modulation of the harmonics yield survives for both cases of pulse shapes. We plot the yield of

11th-order harmonics in Fig. 3(c), where such modulations clearly present, but with the number of peaks twice as many as those shown in Fig. 1(b).

The doubling of the slanted fringes and resonance peaks when one sums all the k points is due to the breaking of the reflective symmetry for a given point $k_0 \neq 0$ in the BZ. To explain this symmetry-breaking behavior, we choose the electron starting from a point $k_0 \neq 0$ and add up all the interband current according to Eq. (14). For a monochromatic pulse, the tunneling points can be expressed as $\{t_{s1} + lT, t_{s2} + lT\}$ with a period of T, $l \in \mathbb{Z}$, as shown in the inset of Fig. 3(c). Similar to $k_0 = 0$ case, the result of the geometric series is the sum of two quasiperiodic terms: by a time translation of one optical cycle, the first term changes a phase of $\int_0^T E_{cv}[k_0 + A(t)]dt$ and the second term remains the same. This leads to harmonics of frequency $\omega = l\omega_0$ and the intensity-dependent peaks at $\omega = l\omega_0 + \Omega_v^{(0)}(k_0) - \Omega_c^{(0)}(k_0)$. By choosing $k_0' = -k_0$, it can be found that $j_{\text{inter}}(t; k_0) = -j_{\text{inter}}(t + T/2; -k_0)$; thus, for the second term, one has

$$\begin{aligned} & j_{\text{inter}}^{(2)}(t; k_0) + j_{\text{inter}}^{(2)}(t; -k_0) \\ & \quad = -j_{\text{inter}}^{(2)}(t + T/2; k_0) + j_{\text{inter}}^{(2)}(t + T; -k_0) \\ & \quad = -j_{\text{inter}}^{(2)}(t + T/2; k_0) - j_{\text{inter}}^{(2)}(t + T/2; -k_0), \end{aligned} \quad (16)$$

which changes a sign by a time translation of $T/2$. This means that the even-order harmonics will vanish due to the interference between radiations emitted by electrons starting from the k_0 and $-k_0$ points.

However, there is no such cancellation for the first term in the interband current, which results in the slanted fringes spaced by one photon energy. With a similar analysis, we can get the resonance condition of population transfer,

$$E_0 + U_p \equiv \overline{E_c - E_v} = n\omega_0, \quad n \in \mathbb{Z}. \quad (17)$$

This phenomenon has become well known as the multiphoton channel-closing effect, both in the atomic systems [44,60,61] and in the solids [12,52,53]. The so-called channel closing shows sharp features, such as a sudden change in the slope of the intensity dependence of the total ionization rate or a sudden yield enhancement in a certain radiation spectral region at particular intensities or wavelengths.

With the different dependence of the quiver motion energy U_p on the field strength between the atomic and solid systems, one expects to see a different behavior in the spectrum. At a given frequency, U_p is proportional to the field intensity I_0 in the atomic case, while to the field strength F_0 for the case of solids, as shown in Fig. 1(a). Therefore, as can be seen from Fig. 3(c), the channel-closing peaks are evenly spaced as a function of A_0. This phenomenon may have shown its footprints in recent experiments [4,54].

C. Results for a two-dimensional model

Many two-dimensional materials have been used to generate the high-order harmonic generation [6,7]. When a laser pulse shines into a bulk solid material, the detected harmonic signals mainly come from the interaction of the laser with the back surface of the material because of the severe reabsorption inside the material [1]. Therefore, it is important to examine whether the observed channel-closing effect exists in a two-dimensional model.

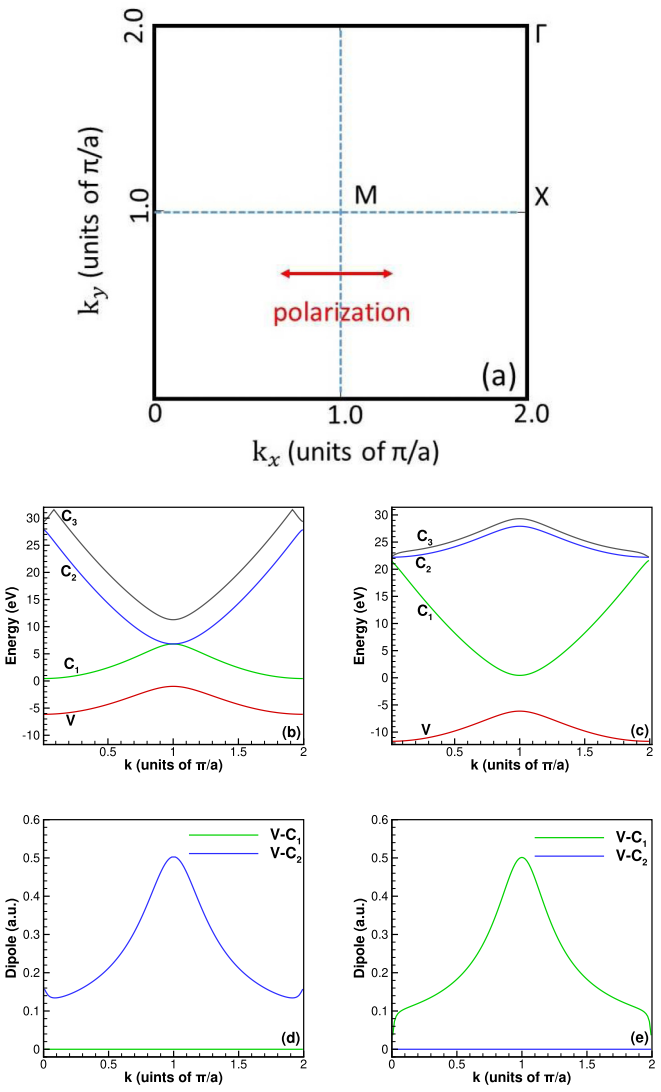

FIG. 4. (a) The Brillouin zone of the 2D model and high-symmetric points in the reciprocal space. The four lowest energy bands are shown along the laser polarization, (b) from $(0, \pi/a)$ to $X(2\pi/a, \pi/a)$ and (c) from (0,0) to $(2\pi/a, 0)$. The corresponding dipoles between the valence and the two lowest conduction bands are shown in (d) and (e), respectively.

For such a purpose, we assume a square unit cell with a side length of a and with a depth $-V_0$. Inside *each cell*, the potential is given by

$$V(x, y) = -V_0 \exp\left[-\alpha \frac{(x - x_0)^2}{a^2} - \alpha \frac{(y - y_0)^2}{a^2}\right], \quad (18)$$

where (x_0, y_0) are the coordinates of the center of this cell. For the calculations presented below, we use the following parameters: $a = 4$ a.u., $V_0 = 1.5\pi^2/2a^2$, and $\alpha = 6.5$ a.u. This model has been previously used [62] to compute HHG in solids.

The band structures of the 2D model are much more complicated than those of the 1D model. However, the essential dynamics of the Bloch electron in the 2D model is very

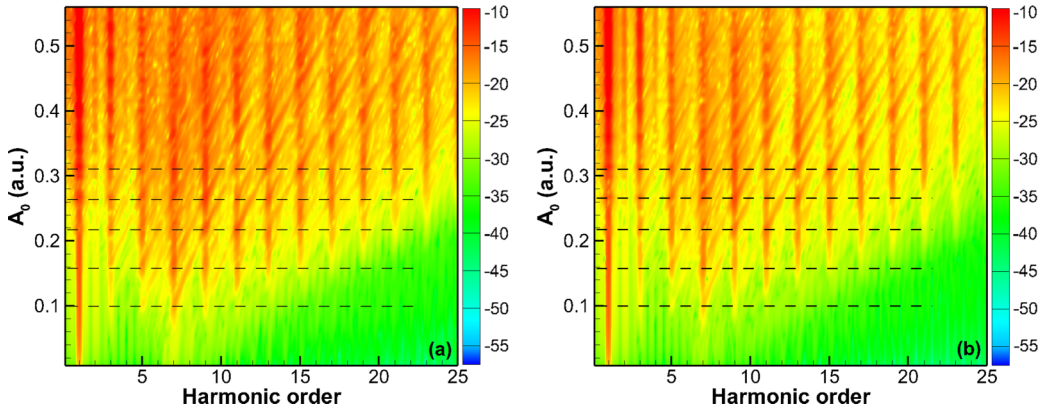

FIG. 5. The HHG spectrum for the 2D model integrated over the full BZ and a single line along the M-X direction from the $(0, 0)$ point are shown in (a) and (b), respectively. An eight-cycle trapezoidal laser pulse is used, with wavelength $\lambda = 1200$ nm ($\omega_0 \approx 0.038$ a.u.), linearly polarized along the M-X direction. The black dashed line indicates the enhanced positions of the channel closing, which are almost at the same values of the vector potential in (a) and (b).

similar to that in the 1D model when a linearly polarized laser is applied, except that the electron is easier to be excited to higher conduction bands and thus to generate multiple plateau structures [24]. In the present work, we solve the corresponding TDSE of the two-dimensional model using the numerical methods adopted in our previous work [24]. To investigate the contributions of the Floquet-Bloch states and channel-closing effects in the 2D model, we use an eight-cycle trapezoidal laser pulse with a wavelength $\lambda = 1200$ nm ($\omega_0 \approx 0.038$ a.u.), polarized along M-X direction, as sketched in Fig. 4(a).

From the discussions of the 1D model, we learn that the harmonic spectrum from a single k point shows strong contributions from the Floquet-Bloch states, with the presence of slanted curves spaced by $2\omega_0$. If one considers the contributions from all k points in the BZ, the spacing of the slanted curves changes from $2\omega_0$ to $1\omega_0$ due to the symmetry breaking, which is similar to the channel-closing effect in the atomic ionization. Due to the above consideration, for the 2D model case, we first need to identify the point where the tunneling probability is the largest if we want to examine the channel-closing effect in the 2D model.

Not as simple as the case of the 1D model, we find that the point with the largest tunneling probability is not the symmetry center such as $M(\pi/a, \pi/a)$ or $\Gamma(\pi/2a, \pi/2a)$. Therefore, we calculate the band structures and the dipole transition matrices starting from different points along the laser polarization. Figures 4(b) and 4(d) show those from $(0, \pi/a)$ to $(2\pi/a, \pi/a)$, and Figs. 4(c) and 4(e) show those from (0,0) to $(2\pi/a, 0)$. As one can see, the minimum band gap of V-C_1 in Fig. 4(b) occurs when $k = 0$. However, the transition dipole of V-C_1 along the polarization direction is zero, so the tunneling can only occur between V-C_2. On the contrary, the smallest band gap of V-C_1 in Fig. 4(d) occurs when $k = \pi/a$, and the energy of the band gap is the same with that of the $k = 0$ point in Fig. 4(b). But in this case, the tunneling can occur between V-C_1 with the largest probability sitting at the point of $k = \pi/a$, as is clearly shown in Fig. 4(e).

Now we can make a comparison between the harmonic spectra calculated, respectively, for all the points in the full BZ and along a line starting from the $(0, 0)$ point. The results are presented in Figs. 5(a) and 5(b), which show only a little difference and indicate that the HHG is dominated by the central line along the polarization direction. This can be understood by another saddle-point condition for Eq. (A12): for a line along the polarization direction with spacing $\Delta k_y \ll \pi/a$, the y component of integration in Eq. (A12) is

$$\int_{t_s}^{t} \frac{\partial E_{cv}}{\partial k_y}[k_x(t), \Delta k_y]dt \approx \Delta k_y \int_{t_s}^{t} \frac{\partial^2 E_{cv}}{\partial k_y^2}[k_x(t), 0]dt. \quad (19)$$

Since $\partial^2 E_{cv}/\partial k_y^2$ does not change its sign in this region, this condition can never be satisfied for $\Delta k_y \neq 0$. Although it may not be true when Δk_y is not so small, the minimum-energy gap will increase and the tunneling probability will dramatically decrease. Thus, we can conclude that only the central line in the BZ contributes to the HHG over the full BZ. Similar analysis can be made for models with a higher dimension.

Finally, we address one of the experimental issue for the observation, i.e., the laser-focusing volume effects. When the laser shines on the solid materials, a large number of crystal lattices are exposed to the laser fields, but with different effective field strengths. Therefore, the important question is whether one can experimentally observe the resonance effects in the harmonic yield. For the present 2D model, we consider this issue by a focusing volume averaging [63]:

$$Y(I_0) = \int_0^{I_0} \frac{Y(A)}{I} dI, \quad (20)$$

where I_0 is the peak intensity in the focusing volume, and $\frac{1}{I}$ approximately simulates the distribution of the laser intensities inside the volume. $Y(I)$ is the intensity of the harmonic signal corresponding to the intensity I for all the k points in the BZ. In Fig. 6, for the case of the trapezoidal envelope at the wavelength of 1200 nm, we show the harmonic yield for the first plateau region (about 7th–15th order of harmonics) after the averaging processes (blue dashed line). It is almost the same with the structure of a certain order harmonic in the first plateau range. As we can see, although the oscillation structure is largely smoothed, the curve does show step structures. We point out that there may exist footprints of these step structures in recent experimental measurements

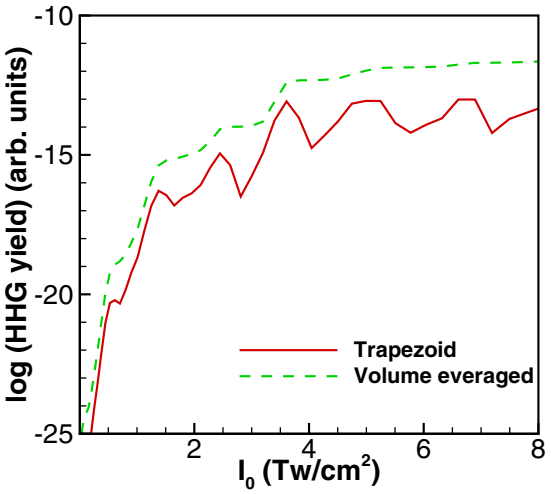

FIG. 6. The yield of the first platform (7–15 order) from the 2D model case with all k points from 2D momentum space. The blue dashed line is the averaged result after considering the laser-focusing volume effects for the trapezoidal envelope.

[1,6,28,42], but with only a few discussions on this effect [54]. The channel-closing effect of HHG in solids may be more easily observed by using materials with a large energy gap such as Al_2O_3 [28] and SiO_2 [3], by adopting a driving laser in the near-infrared region.

V. CONCLUSIONS

In conclusion, we have numerically identified a set of intensity-dependent structures in the harmonic generation in solids, which is caused by transitions between different field-dressed states. An overall enhancement of the harmonic yield can be observed, as an analog to the channel-closing effect in atomic systems. We showed that the currently observed phenomena can be understood in the framework of Floquet-Bloch states and with the strong-field approximation. Our analysis is confined to the region where $\omega_0/\Delta \ll 1$, $\sqrt{m^*\Delta^3}/F \gg 1$ and the amplitude of the vector potential is comparable to the reciprocal lattice vector. Actually, most previous experiments have been carried out in this region. The channel-closing effect in solids will lead to a nonmonotonic increase of the harmonic yield as a function of the laser intensity. After a rough consideration of the laser-focusing volume effects, these resonances can survive as a steplike structure, which may have shown their footprints in several recent experimental measurements.

ACKNOWLEDGMENTS

This work is supported by the National Natural Science Foundation of China (NSFC) under Grants No. 11574010 and No. 11725416 and by the National Key R&D Program of China (Grant No. 2018YFA0306302).

APPENDIX: EVALUATION FOR SADDLE POINTS

In this Appendix, we show how to estimate the integral with saddle points and how to solve the saddle-point equation (12). We rewrite Eq. (11) into

$$\begin{aligned} & a_v(t)e^{i\phi_v(t)} \\ &= -i\int_{-\infty}^{t} \partial_\tau A(\tau)\cdot\langle\Psi_c(k)|\nabla_k|\Psi_v(k)\rangle e^{-i\phi_{cv}(\tau)}d\tau \\ &= -i\int^{k(t)} \langle\Psi_c(k)|\nabla_k|\Psi_v(k)\rangle e^{-i\phi_{cv}(\tau)}dk. \end{aligned} \tag{A1}$$

By rewriting $\langle\Psi_c(k)|\nabla_k|\Psi_v(k)\rangle$ into $\langle\Psi_c^*(-k)|\nabla_k|\Psi_v(k)\rangle$, we can extend k from the real axis into the complex plane (with a branch cut between each half optical cycle). According to Keldysh's work [64], the integrand has a pole at the saddle point,

$$\langle\Psi_c^*(-k)|\nabla_k|\Psi_v(k)\rangle = \frac{i}{4(k-q)} + \cdots, \tag{A2}$$

where $E_c(q) - E_v(q) = 0$. So, the integration can be done with the residue method if one changes the upper bound t to the end of the pulse,

$$a_v(t)e^{i\phi_v(t)}|_{t=\infty} = \frac{\pi}{2}\sum_{t_s} \mathrm{sgn}[F(t_s)\xi_{cv}]e^{-i\phi_{cv}(t_s)}, \tag{A3}$$

where the sign function corresponds to the different direction of integral contour. For a finite t, the residue method is not applicable since we cannot just use a large semicircle to construct a close contour. However, here we just take the poles with the real part less than t to approximate the integration. Nevertheless, in doing so, the step functionlike behavior will overestimate the HHG yield in the high-frequency region, as discussed in the main text.

Now we consider how to solve the saddle-point equation. Since the tunneling process always takes place near the minimal band gap, we use the simple expression $E_c(k) - E_v(k) \approx \sqrt{\Delta^2 + v^2k^2}$ to approximate the gap energy, where Δ is the minimum band gap between the bands c and v. The parameter v is related to the effective mass of the electron-hole pair with $m^* = \Delta/v^2$. Thus the saddle point happens to be $q = \pm i\Delta/v$. For a monochromatic pulse with $A(t) = A_0\cos\omega_0 t$, one has

$$k_0 + A_0\cos\omega_0 t_r \cosh\omega_0 t_i = 0, \tag{A4}$$

$$\mp vA_0\sin\omega_0 t_r \sinh\omega_0 t_i = \Delta. \tag{A5}$$

The solution to the above equations is given by

$$\omega_0 t_r = 2l\pi \pm \arcsin\sqrt{\frac{\sqrt{u^2+4\Delta^2v^2A_0^2}-u}{2v^2A_0^2}}, \tag{A6}$$

$$\omega_0 t_i = \mathrm{arcsinh}\sqrt{\frac{\sqrt{u^2+4\Delta^2v^2A_0^2}+u}{2v^2A_0^2}}, \tag{A7}$$

where $u = \Delta^2 + v^2(k_0^2 - A_0^2)$ and $l \in \mathbb{Z}$. For other types of pulse envelopes, it is difficult, if possible, to find an analytic solution to saddle points. However, the Newton-Raphson method can be applied to find roots. The complex action can be evaluated as follows:

$$\begin{aligned} \Delta\phi(t_s) &= \Delta\phi(t_r) + \Delta\phi(t_s) - \Delta\phi(t_r) \\ &\approx \Delta\phi(t_r) + i\int_0^{t_i} \sqrt{\Delta^2 + v^2[k_0 + A(t_r + is)]^2}ds. \end{aligned} \tag{A8}$$

The integration can be numerically carried out by the second type of Gauss-Chebyshev quadrature.

It is interesting to consider the limit case where $\omega_0 \to 0, A_0 \to \infty$ but $\omega_0 A_0$ keeps finite, which corresponds to the classical Landau-Zener tunneling. In this limit, $\omega_0 t_i \approx \Delta/vA_0 \ll 1$ and $\omega_0 t_r \approx \pm\pi$. The imaginary part of the action is

$$\int_0^{t_i} \sqrt{\Delta^2 + v^2[k_0 + A(t_r + is)]^2}ds = \int_0^{t_i} \sqrt{\Delta^2 - v^2A_0^2\omega_0^2 s^2}ds = \frac{\pi\Delta^2}{4v\omega_0 A_0}. \quad \text{(A9)}$$

Therefore, one can finally arrive at a transition rate $(\pi/2)^2 \exp(-\pi\Delta^2/2v\omega_0 A_0)$, which differs from the Landau-Zener formula by a prefactor $(\pi/2)^2$. The difference in an overall prefactor is understandable and it is also common in the strong-field approximation for atomic systems [65]. With this result, one can check the feasibility of our assumption, $|a_c|^2 \ll |a_v|^2$. It requires $\Delta^2/v\omega_0 A_0 \gg 1$ or

$$\sqrt{m^*\Delta^3}/F_0 \gg 1. \quad \text{(A10)}$$

Finally, one may also apply the saddle-point method to approximate the integration of k_0,

$$j_{\rm er}(t) = 2\,\mathrm{Re}\int_{\rm BZ} dk_0\, p_{cv}[k(t)] \sum_{\mathrm{Re}\,t_s<t} \mathrm{sgn}(F) e^{i\phi_{cv}(t_s,t)} \approx 2\,\mathrm{Re}\sum_{k_s,\mathrm{Re}\,t_s<t} \sqrt{\frac{2\pi i}{\phi''_{cv}(t_s,t;k_s)}}\, p_{cv}[k_s + A(t)] \times \mathrm{sgn}[F(t_s)] e^{i\phi_{cv}(t_s,t;k_s)}, \quad \text{(A11)}$$

where k_s satisfies

$$\mathrm{Re}\,\frac{d}{dk_0}\phi_{cv}[t_s(k_0), t; k_0]|_{k_0=k_s} = \mathrm{Re}\int_{t_s}^{t} \frac{\partial E_{cv}}{\partial k} dt = 0, \quad \text{(A12)}$$

with ϕ''_{cv} being the second-order derivative of k_0.

[1] S. Ghimire, A. D. DiChiara, E. Sistrunk, P. Agostini, L. F. DiMauro, and D. A. Reis, Nat. Phys. **7**, 138 (2011).
[2] O. Schubert, M. Hohenleutner, F. Langer, B. Urbanek, C. Lange, U. Huttner, D. Golde, T. Meier, M. Kira, S. W. Koch, and R. Huber, Nat. Photon. **8**, 119 (2014).
[3] T. T. Luu, M. Garg, S. Y. Kruchinin, A. Moulet, M. T. Hassan, and E. Goulielmakis, Nature (London) **521**, 498 (2015).
[4] G. Ndabashimiye, S. Ghimire, M. Wu, D. A. Browne, K. J. Schafer, M. B. Gaarde, and D. A. Reis, Nature (London) **534**, 520 (2016).
[5] M. Hohenleutner, F. Langer, O. Schubert, M. Knorr, U. Huttner, S. W. Koch, M. Kira, and R. Huber, Nature (London) **523**, 572 (2015).
[6] H. Liu, Y. Li, Y. S. You, S. Ghimire, T. F. Heinz, and D. A. Reis, Nat. Phys. **13**, 262 (2017).
[7] N. Yoshikawa, T. Tamaya, and K. Tanaka, Science **356**, 736 (2017).
[8] P. Bowlan, E. Martinez-Moreno, K. Reimann, T. Elsaesser, and M. Woerner, Phys. Rev. B **89**, 041408(R) (2014).
[9] G. P. Zhang, M. S. Si, M. Murakami, Y. H. Bai, and T. F. George, Nat. Commun. **9**, 3031 (2018).
[10] M. Wu, S. Ghimire, D. A. Reis, K. J. Schafer, and M. B. Gaarde, Phys. Rev. A **91**, 043839 (2015).
[11] M. Wu, D. A. Browne, K. J. Schafer, and M. B. Gaarde, Phys. Rev. A **94**, 063403 (2016).
[12] L. V. Keldysh, Sov. Phys. JETP **20**, 1307 (1965).
[13] J. B. Krieger and G. J. Iafrate, Phys. Rev. B **33**, 5494 (1986).
[14] Y. A. Bychkov and A. M. Dykhne, Sov. Phys. JETP **31**, 928 (1970).
[15] D. Bauer and K. K. Hansen, Phys. Rev. Lett. **120**, 177401 (2018).
[16] C. Yu, S. Jiang, and R. Lu, Advances in Physics: X **4**, 1562982 (2019).
[17] O. D. Mücke, Phys. Rev. B **84**, 081202(R) (2011).
[18] G. Vampa, C. R. McDonald, G. Orlando, D. D. Klug, P. B. Corkum, and T. Brabec, Phys. Rev. Lett. **113**, 073901 (2014).
[19] C. R. McDonald, G. Vampa, P. B. Corkum, and T. Brabec, Phys. Rev. A **92**, 033845 (2015).
[20] G. Vampa, C. R. McDonald, G. Orlando, P. B. Corkum, and T. Brabec, Phys. Rev. B **91**, 064302 (2015).
[21] P. G. Hawkins, M. Y. Ivanov, and V. S. Yakovlev, Phys. Rev. A **91**, 013405 (2015).
[22] D. Golde, T. Meier, and S. W. Koch, Phys. Rev. B **77**, 075330 (2008).
[23] T.-Y. Du and X.-B. Bian, Opt. Express **25**, 151 (2017).
[24] J.-Z. Jin, X.-R. Xiao, H. Liang, M.-X. Wang, S.-G. Chen, Q. Gong, and L.-Y. Peng, Phys. Rev. A **97**, 043420 (2018).
[25] J. D. Cox, A. Marini, and F. J. G. de Abajo, Nat. Commun. **8**, 14380 (2016).
[26] F. Langer, M. Hohenleutner, U. Huttner, S. W. Koch, M. Kira, and R. Huber, Nat. Photon. **11**, 227 (2017).
[27] Y. S. You, Y. Yin, Y. Wu, A. Chew, X. Ren, F. Zhuang, S. Gholam-Mirzaei, M. Chini, Z. Chang, and S. Ghimire, Nat. Commun. **8**, 724 (2017).
[28] H. Kim, S. Han, Y. W. Kim, S. Kim, and S. W. Kim, ACS Photon. **4**, 1627 (2017).
[29] N. Tancogne-Dejean and A. Rubio, Sci. Adv. **4**, eaao5207 (2018).
[30] N. Tancogne-Dejean, O. D. Mücke, F. X. Kärtner, and A. Rubio, Phys. Rev. Lett. **118**, 087403 (2017).
[31] M. Wu, Y. You, S. Ghimire, D. A. Reis, D. A. Browne, K. J. Schafer, and M. B. Gaarde, Phys. Rev. A **96**, 063412 (2017).
[32] T. T. Luu and H. J. Wörner, Phys. Rev. B **94**, 115164 (2016).
[33] L. Li, P. Lan, X. Zhu, T. Huang, Q. Zhang, M. Lein, and P. Lu, Phys. Rev. Lett. **122**, 193901 (2019).
[34] H. Shirai, F. Kumaki, Y. Nomura, and T. Fuji, Opt. Lett. **43**, 2094 (2018).
[35] F. H. M. Faisal and R. Genieser, Phys. Lett. A **141**, 297 (1989).
[36] O. E. Alon, V. Averbukh, and N. Moiseyev, Adv. Quantum Chem. **47**, 393 (2004).
[37] D. Dimitrovski, T. G. Pedersen, and L. B. Madsen, Phys. Rev. A **95**, 063420 (2017).

[38] Y. Mizumoto, Y. Kayanuma, A. Srivastava, J. Kono, and A. H. Chin, Phys. Rev. B **74**, 045216 (2006).
[39] A. K. Gupta, O. E. Alon, and N. Moiseyev, Phys. Rev. B **68**, 205101 (2003).
[40] S. T. Park, Phys. Rev. A **90**, 013420 (2014).
[41] Y. H. Wang, H. Steinberg, P. Jarillo-Herrero, and N. Gedik, Science **342**, 453 (2013).
[42] G. Vampa, B. G. Ghamsari, S. Siadat Mousavi, T. J. Hammond, A. Olivieri, E. Lisicka-Skrek, A. Y. Naumov, D. M. Villeneuve, A. Staudte, P. Berini, and P. B. Corkum, Nat. Phys. **13**, 659 (2017).
[43] J.-Z. Jin, H. Liang, X.-R. Xiao, M.-X. Wang, S.-G. Chen, X.-Y. Wu, Q. Gong, and Liang-You Peng, J. Phys. B: At. Mol. Opt. Phys. **51**, 16LT01 (2018).
[44] R. Kopold, W. Becker, M. Kleber, and G. G. Paulus, J. Phys. B: At. Mol. Opt. Phys. **35**, 217 (2002).
[45] U. Fano, Phys. Rev. **124**, 1866 (1961).
[46] F. H. M. Faisal and J. Z. Kamiński, Phys. Rev. A **56**, 748 (1997).
[47] S.-I. Chu and D. A. Telnov, Phys. Rep. **390**, 1 (2004).
[48] M. Lewenstein, P. Balcou, M. Y. Ivanov, A. L'Huillier, and P. B. Corkum, Phys. Rev. A **49**, 2117 (1994).
[49] G. Sansone, C. Vozzi, S. Stagira, and M. Nisoli, Phys. Rev. A **70**, 013411 (2004).
[50] R. Kopold, D. B. Milošević, and W. Becker, Phys. Rev. Lett. **84**, 3831 (2000).
[51] D. B. Milošević and W. Becker, Phys. Rev. A **66**, 063417 (2002).
[52] M. S. Wismer, S. Y. Kruchinin, M. Ciappina, M. I. Stockman, and V. S. Yakovlev, Phys. Rev. Lett. **116**, 197401 (2016).
[53] T. Paasch-Colberg, S. Y. Kruchinin, Ö. Sağlam, S. Kapser, S. Cabrini, S. Muehlbrandt, J. Reichert, J. V. Barth, R. Ernstorfer, R. Kienberger, V. S. Yakovlev, N. Karpowicz, and A. Schiffrin, Optica **3**, 1358 (2016).
[54] T.-Y. Du, D. Tang, and X.-B. Bian, Phys. Rev. A **98**, 063416 (2018).
[55] T.-Y. Du and S.-J. Ding, Phys. Rev. A **99**, 033406 (2019).
[56] X. Liu, X. Zhu, X. Zhang, D. Wang, P. Lan, and P. Lu, Opt. Express **25**, 29216 (2017).
[57] G. Ernotte, T. J. Hammond, and M. Taucer, Phys. Rev. B **98**, 235202 (2018).
[58] K. K. Hansen, T. Deffge, and D. Bauer, Phys. Rev. A **96**, 053418 (2017).
[59] J. Li, S. Fu, H. Wang, X. Zhang, B. Ding, B. Hu, and H. Du, Phys. Rev. A **98**, 043409 (2018).
[60] H. R. Reiss, Phys. Rev. A **22**, 1786 (1980).
[61] D. B. Milošević, E. Hasović, M. Busuladžić, A. Gazibegović-Busuladžić, and W. Becker, Phys. Rev. A **76**, 053410 (2007).
[62] G.-R. Jia, X.-Q. Wang, T.-Y. Du, X.-H. Huang, and X.-B. Bian, J. Chem. Phys. **149**, 154304 (2018).
[63] P. Hansch, M. A. Walker, and L. D. Van Woerkom, Phys. Rev. A **54**, R2559(R) (1996).
[64] L. V. Keldysh, Sov. Phys. JETP **6**, 763 (1958).
[65] D. B. Milošević, G. G. Paulus, D. Bauer, and W. Becker, J. Phys. B: At. Mol. Opt. Phys. **39**, R203 (2006).